A combined experimental and numerical approach to the assessment of floc settling velocity using fractal geometry

R. B. Moruzzi, J. Bridgeman and P. A. G. Silva

ABSTRACT

Sedimentation processes are fundamental to solids/liquid separation in water and wastewater treatment, and therefore a robust understanding of the settlement characteristics of mass fractal aggregates (flocs) formed in the flocculation stage is fundamental to optimized settlement tank design and operation. However, the use of settling as a technique to determine aggregates' traits is limited by current understanding of permeability. In this paper, we combine experimental and numerical approaches to assess settling velocities of fractal aggregates. Using a non-intrusive *in situ* digital image-based method, three- and two-dimensional fractal dimensions were calculated for kaolin-based flocs. By considering shape and fractal dimension, the porosity, density and settling velocities of the flocs were calculated individually, and settling velocities compared with those of spheres of the same density using Stokes' law. Shape analysis shows that the settling velocities for fractal aggregates may be greater or less than those for perfect spheres. For example, fractal aggregates with floc fractal dimension, $D_f = 2.61$, floc size, $d_f > 320$ μm and $d_p = 7.5$ μm settle with lower velocities than those predicted by Stokes' law; whilst, for $D_f = 2.33$, all aggregates of $d_f > 70$ μm and $d_p = 7.5$ μm settled below the velocity calculated by Stokes' law for spheres. Conversely, fractal settling velocities were higher than spheres for all the range of sizes, when D_f of 2.83 was simulated. The ratio of fractal aggregate to sphere settling velocity (the former being obtained from fractal porosity and density considerations), varied from 0.16 to 4.11 for aggregates in the range of 10 and 1,000 μm, primary particle size of 7.5 μm and a three-dimensional fractal dimension between 2.33 and 2.83. However, the ratio decreases to the range of 0.04–2.92 when primary particle size changes to 1.0 μm for the same fractal dimensions. Using the floc analysis technique developed here, the results demonstrate the difference in settlement behaviour between the approach developed here and the traditional Stokes' law approach using solid spheres. The technique and results demonstrate the improvements in understanding, and hence value to be derived, from an analysis based on fractal, rather than Euclidean, geometry when considering flocculation and subsequent clarification performance.

Key words | density, flocculation, fractal dimension, porosity, settling velocity

R. B. Moruzzi (corresponding author)
P. A. G. Silva
UNESP – Universidade Estadual Paulista,
Instituto de Geociências e Ciências Exatas,
Rio Claro, São Paulo,
Brazil
E-mail: *rodrigo.moruzzi@unesp.br*

J. Bridgeman
Faculty of Engineering & Informatics,
University of Bradford,
Bradford,
United Kingdom

INTRODUCTION

Coagulation and flocculation are critical steps in drinking water treatment. During coagulation, a coagulant (e.g. aluminium sulphate) is added to the water to neutralize the negatively charged suspended particles, following which shear-induced interactions generated by slow mixing in a flocculator cause their aggregation into mass fractal aggregates (flocs). Clarification processes in water treatment are often based on sedimentation of flocs. In order to optimize sedimentation, it is important to gain a fundamental understanding of floc settling behaviour. Traditional approaches have used Stokes' law with its inherent assumptions of solid, spherical particles. Flocs are clearly far more complex in structure and behaviour and, therefore, it is important that the impacts of these features of flocs are understood in order that their settling behaviour can be assessed and so predicted with accuracy.

doi: 10.2166/wst.2020.171

Floc aggregation is a dynamic process where mass, surface area, number, and morphology change as functions of the shear stress and time. Furthermore, whilst aggregates may have the same size, they may exhibit different structures due to different particle arrangements during aggregation. The variations in mass, surface area and concentration substantially affect floc behaviour, particularly with regard to collision and to aggregation efficiency (Vahedi & Gorczyca 2012).

Therefore, the irregular shape and porous structure of fractal aggregates may oppose the predicted settling rate using solid spheres. These traits may affect aggregates' density and porosity and hence the drag forces on the floc surface, making velocities (and hydraulic loading rates) slower than the ones predicted by Stokes' law (Vahedi & Gorczyca 2012; Chakraborti & Kaur 2014). This may potentially have influences on the predicted clarification efficiency of settling units, resulting in more solids being dragged out from the tank into the subsequent filters, which may not be designed for such extra loads. Hence, the correct prediction of aggregates' settling rates is crucial for the accurate design of sedimentation tanks and subsequent filters in a full-scale water treatment plant.

Fractal geometry has been extensively used to characterize non-uniform objects and its application to sedimentation will be described below, after a brief description of its main characteristic.

FRACTAL GEOMETRY

Fractals may be described as objects that demonstrate self-similarity (i.e. the existence of the same pattern irrespective of viewing magnification). They can be expressed via a power law relationship comprising two variables, and characterized by non-integer fractal dimensions, as shown in Equations (1)–(3):

$$A \propto L^{D_f} \tag{1}$$

and:

$$V \propto A^{D_f} \tag{2}$$

where V, A and L refer to fractal volume, area and length respectively, whilst D_f is the floc fractal dimension.

In the case of flocs:

$$M \propto L^{D_f} \tag{3}$$

where M refers to floc mass.

Gregory (2009) described flocs as mass fractal objects and found that their fractal structure has important practical implications for floc density. Indeed, several factors affect flocs' fractal structure, including mixer device (Logan & Kilps 1995) and coagulation (Xu *et al.* 2010, 2011), as floc strength is a function of the formation process (He *et al.* 2012). Gregory (2009) found that aggregates formed by perikinetic flocculation display lower fractal dimension than those formed during orthokinetic flocculation, whilst aggregates formed during sweep coagulation are of larger size and fractal dimension compared with those formed during charge neutralization (Kim *et al.* 2001; Li *et al.* 2006).

Fractal aggregates, when densely compacted, are close to Euclidean objects and so have a large fractal dimension ($D_f \sim 2$, for two-dimensional objects), whereas smaller fractal dimensions result from highly branched structures. It is believed that these more compact aggregates, rather than those exhibiting large overall size, exhibit enhanced performance during sedimentation given that the floc settling velocity depends on the aggregate size and fractal dimension (Johnson *et al.* 1996; Gregory 1997; Chakraborti *et al.* 2000; Vahedi & Gorczyca 2012), as shown in Equation (4):

$$v_{st} = \frac{1}{18}\theta g \frac{\rho_p - \rho_w}{\mu} d_{50}^{3-D_f} \frac{d^{D_f-1}}{1 + 0.15\mathrm{Re}^{0.687}}\phi \tag{4}$$

where: v_{st} is the settling velocity of an individual floc; g is acceleration due to gravity; μ is dynamic viscosity of water; D_f is the fractal dimension; d is floc size; d_{50} is the median size of particles within a floc (i.e. primary particles); θ is a dimensionless particle shape factor; and ρ_p and ρ_w are the densities of primary particles and water, respectively.

$\phi = \frac{m_3}{m_f^{3/D_f}}$ and represents the size distribution of N primary mono-sized particles of diameter d_p in a floc, as shown in Equations (5) and (6), where:

$$m_3 = \left(\sum_{i=1}^{N} d_{pi}^3\right)/N \tag{5}$$

and:

$$m_f = \left(\sum_{i=1}^{N} d_{pi}^{D_f}\right)/N \tag{6}$$

The particle Reynolds number is given by Equation (7):

$$\mathrm{Re} = \frac{v_{st} d}{\upsilon} \tag{7}$$

where υ is the kinematic viscosity of water.

Bache *et al.* (1999) found that the floc effective density (ρ_e), given by $\rho_e = \rho_e - \rho_w$, is related to floc size (d) via Equation (8):

$$\rho_e = A d^{-n} \tag{8}$$

where: A is a packing factor and is a function of coagulant dose and coagulation pH; and n is a coefficient that is a function of D_f. For aluminium floc and humic substances, the value of n varies from 1.8 to 2.0.

Considering the importance of structural and morphological characteristics of fractal aggregates, the objective of the work reported in this paper is to investigate the porosity and density of aggregates after flocculation based on their fractal dimension calculated individually, measured by a non-intrusive image-analysis-based method, in order to inform our understanding of floc sedimentation and so improve clarification performance.

METHODS

Suspensions

Suspensions were prepared in the laboratory from a kaolinite solution following Yukselen & Gregory (2004) to obtain a turbidity of 25 NTU. The kaolinite was characterized by scanning electron microscopy (SEM) using a JEOL JSM-6010LA microscope coupled to an X-ray spectrometer and via laser granulometry using the Malvern Mastersizer 2000 to obtain composition and mean grain size. The suspension was coagulated with commercial aluminium sulphate, and the pH was adjusted with a 1 M sodium hydroxide solution. The optimum coagulation conditions identified by de Oliveira *et al.* (2015) using the same synthetic water were adopted, i.e., 2 mg $Al^{+3} \cdot L^{-1}$, pH 7.5. Flocculation was performed with mean velocity gradients ($\overline{G_f}$) of 20–60 s^{-1}, which were determined by torque measurements, for flocculation times of 15 min to obtain flocs of different sizes and shapes.

Data acquisition

A total of 1,000 floc images were captured immediately post-flocculation (high-speed Miro EX-4 camera with interchangeable lenses, sampling at 25 Hz for 40 s). Image resolution was 800×600 pixels with a visual field of 6×8 mm. Shutter speed was set to 800 μs and pixel size was 10 μm. Illumination was via a collimated laser beam modified by a cylindrical lens for plane dispersion with a thickness of 2 mm (following Moruzzi *et al.* 2017) placed perpendicular to the focus direction. Nominal laser power was 2,000 mW, producing light at a wavelength of 532 nm (green). A schematic of the experimental apparatus is shown in Figure 1.

Digital images were processed using Image Pro Plus 7.0 software. The images were transformed into binary matrices

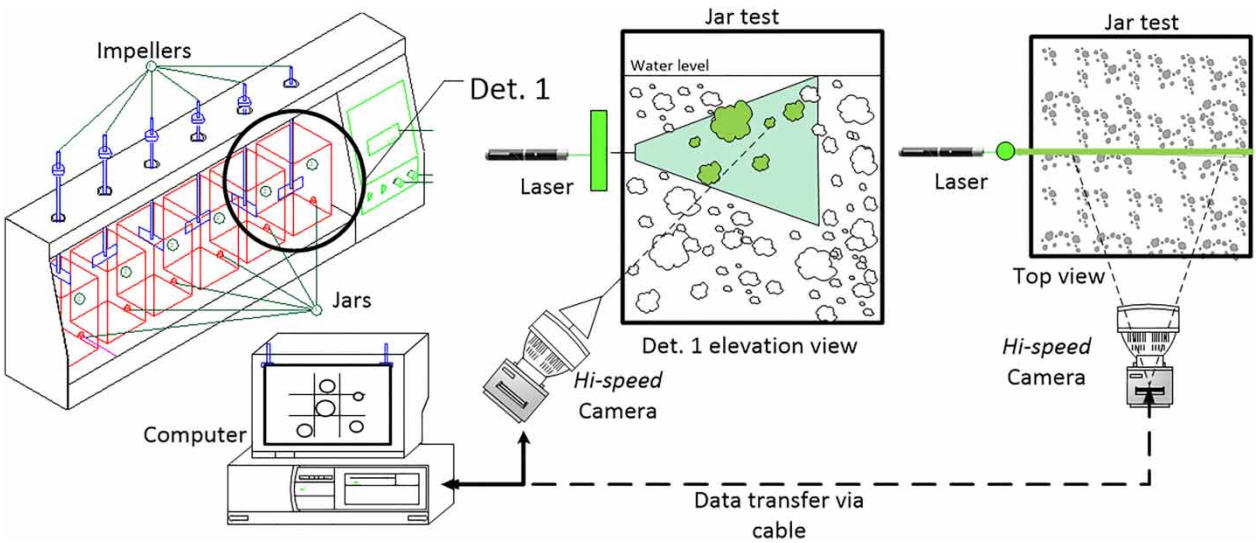

Figure 1 | Scheme of the experimental apparatus. Adapted from Moruzzi *et al.* (2017).

by the segmentation process using a degree of 128/256 as the threshold and were then subjected to the particle image velocimeter (PIV) processing of the same package. Area and Diameter (max) of each floc were used to track each aggregate, with cut-off values of 200 pixels respectively (Chakraborti *et al.* 2003). In total, 118 aggregates were selected, for which the attributes of interest (Diameter (max), Diameter (min), Diameter (mean), Area, Y coordinate, and Perimeter) were obtained. Further details on data acquisition and treatment can be found in Moruzzi *et al.* (2017, 2019).

Determination of fractal characteristics

The value of D_f and the shape parameter, b, for each aggregate can be obtained from linear regression of the experimental data in the linearized form of Equation (9) (i.e. Equation (10)). Here, the slope of the straight line corresponds to the exponent (D_f) and the intercept corresponds to the shape parameter b:

$$N = b\left[\frac{d_f}{d_p}\right]^{D_f} \tag{9}$$

$$\ln N = \ln b + D_f \ln\left[\frac{d_f}{d_p}\right] \tag{10}$$

where: D_f is the three-dimensional fractal dimension; d_p is the primary particle diameter (m); d_f is the floc diameter (m); N is the number of primary particles of diameter d_p per volume of floc of diameter d_f; and b is the shape parameter, defined as:

$$b = \left(\frac{\zeta \cdot \xi}{\xi_0}\right)^{D_f/3} \tag{11}$$

where: ζ is the packing factor; ξ is the shape factor; and ξ_0 is the primary particle shape factor.

The number of primary particles per unit of aggregate volume, N, was determined by rotation of the ellipsoid about the x-axis of the ellipsoid fitted to the highest and lowest dimensions determined by the image analyses, as illustrated in Figure 2 and Equations (12) and (13), following Chakraborti *et al.* (2000):

$$E = \left\{(x,\ y,\ z) \in \mathrm{R}^3 : \frac{x^2}{a^2} + \frac{y^2}{b^2} + \frac{z^2}{c^2} \le 1, a > 0,\ b > 0\ \&\ c > 0\right\} \tag{12}$$

$$V(E) = \iiint_E \left(\frac{\partial A}{\partial x} + \frac{\partial B}{\partial y} + \frac{\partial C}{\partial z}\right) dx.dy.dz = \iint_S z.dx.dy \tag{13}$$

where: A, B, and C are the integration limits of the a, b, and c axes of the ellipsoid (E) with volume $V(E)$; and S is the surface of the ellipsoid (E).

With these data, the value of the three-dimensional fractal dimension (D_{fp}) was obtained for the set of aggregates by fitting the volumes to Equation (14) in the linearized form:

$$V \sim d_{max}^{D_{fp}} \tag{14}$$

where: V is the volume of the ellipsoid containing the floc (m^3); and d_{max} is the largest dimension of the floc (m).

The two-dimensional fractal dimension (D_{fp}') for the set of aggregates was determined using Equation (15), and the ratio of D_{fp}: D_{fp}' for the data set was then used to calculate the three-dimensional fractal dimension per aggregate according to Equation (16). The value of d_p in Equation (16) was assumed from the kaolin volume distribution, adopting mono-sized primary particles as simplification for the D_f calculation.

$$A \sim d_{max}^{D_{fp}'} \tag{15}$$

where: A is the projected floc area on the image plane; and

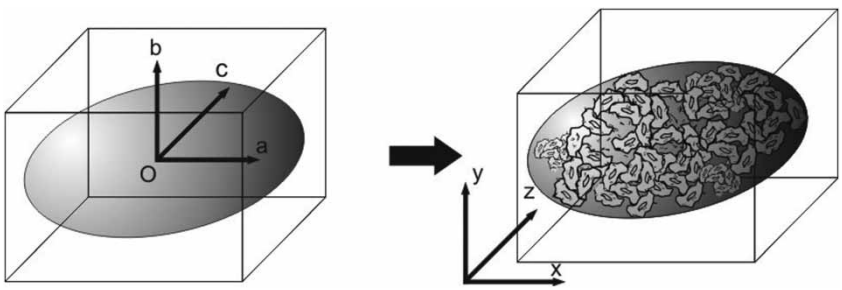

Figure 2 | Example of aggregate encased in ellipsoid.

D_{fp}' is the two-dimensional fractal dimension.

$$D_f = \frac{D_{fp}}{D_{fp}'}\left(\frac{\ln N}{\ln\left(\frac{d_{max}}{d_p}\right)}\right) \quad (16)$$

With the shape, floc dimension, particle dimension, and three-dimensional fractal dimension parameters calculated per particle, the floc porosity and density were determined with Equations (17) and (18), considering a mass balance between the floc, the particle, and the voids occupied by the liquid.

The porosity of the floc, ε_f, with diameter d_f was determined via:

$$\varepsilon_f = 1 - (b.d_f^{D_f-3}.d_p^{3-D_f}) \quad (17)$$

and the floc density, ρ_f, via:

$$\rho_f = \rho_l + (b.d_f^{D_f-3}.d_p^{3-D_f}(\rho_p - \rho_l)) \quad (18)$$

where: ρ_f is the floc density (kg·m^{-3}); ρ_l is the density of water (kg·m^{-3}); and ρ_p is the density of the primary particles (kg·m^{-3}).

Settling velocity

The density, floc porosity, and three-dimensional fractal dimension were used to evaluate the sedimentation velocities of Euclidean geometry spheres (V_{sphere}) and fractals ($V_{fractal}$). It was assumed that the floc dimensions did not change during sedimentation. For this purpose, the Newton equation (Equation (19)) in equilibrium ($\Sigma F_y = 0$) was used for the particular case where the dimensionless Reynolds number (Re) <1, such that the drag coefficient can be described according to Equation (20). Thus, V_{sphere} can be described by Equation (21) and $V_{fractal}$ by Equation (22), and they are distinguished from each other in the geometric and density terms of the equations. The geometric term of Equation (22) will always reduce the contribution of size to velocity for fractal aggregates, unless d_f approaches d_p (for $d_f > d_p$), resulting in the square relation of Equation (21) (d_f^2). Finally, the ratio of the velocities was determined for each particle according to Equation (23).

$$V_{sphere} = \sqrt{\frac{4.(\rho_f - \rho_l).g.d_f}{3.\rho_l \cdot C_d}} \quad (19)$$

where: V_{sphere} is the Newton velocity for the Euclidean sphere (m·s^{-1}); g is the acceleration due to gravity (m·s^{-2}); and C_d is the drag coefficient.

Assuming Re < 1,

$$C_d = \frac{24}{Re} = \frac{24\mu}{V_{st}d_f\rho_l} \quad (20)$$

where: Re is the Reynolds number; V is the floc terminal velocity (m·s^{-1}); and μ is the absolute viscosity (N·m^{-2}·s).

Hence:

$$V_{sphere} = \frac{g(\rho_f - \rho_l)d_f^2}{18\mu} \quad (21)$$

Valid for Re < 1 and d_f <1 mm.

$$V_{fractal} = \frac{g(\rho_p - \rho_l)d_f^{D_f-1}d_p^{3-D_f}.b}{18\mu} \quad (22)$$

where $V_{fractal}$ is the velocity based on fractal aggregates with diameter d_f (m·s^{-1}).

The dimensionless quotient of the fractal and Euclidean sphere velocities, Γ, is defined as:

$$\Gamma = \frac{V_{fractal}}{V_{sphere}} \quad (23)$$

RESULTS AND DISCUSSION

Figure 3 shows the kaolinite (Kaolin, Fluka) particle size distribution: 0.4–100 μm in volume with median 7.5 μm and in number (N) with median 1.0 μm, which is in agreement with other studies (Zbik & Smart 1998; Aparicio *et al.* 2004). An example of one scanning electron microscopy image taken from the kaolin dry sample is also presented in detail, showing qualitatively the range of size, shapes and textures of the primary particles. This result supports the definition of the appropriate pixel size for the determination of the smaller cluster of the aggregate, and primary particle size adopted herein as well.

Figure 4 shows a post-flocculation ($G_f = 20\ s^{-1}$, $T_f =$ 15 min) aggregate characterization image. It is clear that any assumption of solid sphericity, and hence use of traditional Stokes' law approach, is inappropriate for representing the shape of the aggregates. Further, the existence of voids within the floc alters the porosity and density of the aggregate, both of which affect floc terminal velocity.

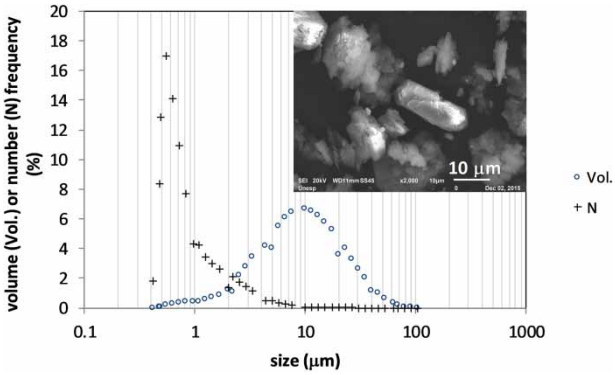

Figure 3 | Kaolin size distribution in number and volume. Scanning electron microscopy (SEM) image detail in the right upper side.

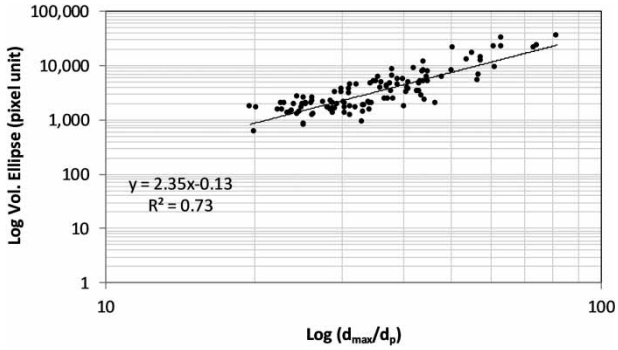

Figure 5 | Determination of three-dimensional fractal dimension from image analysis measurements by means of the log–log plot of volume versus relative longest length based on pixel size.

Figure 5 shows the relationship between log volume of the encased ellipsoid and the log of the ratio of d_{max}:d_p, from which the values $b = 0.78$ and $D_{fp} = 2.35$ were determined (Equation (10)). The value of D_{fp} represents elongated medium aggregates, far from a perfect sphere, and agrees with other studies (Johnson *et al.* 1996; Chakraborti *et al.* 2003; Li *et al.* 2006). Plotting log aggregate area against log (d_{max}/d_p) yielded a two-dimensional fractal dimension, D_{fp}', value of 1.50 (Figure S1, Supplementary Information).

These results were then applied to Equations (16)–(18) to determine the three-dimensional fractal dimension, porosity and density for the flocs.

Table 1 presents descriptive statistics obtained from all the aggregates in terms of the highest dimension (D_{max}), lowest dimension (D_{min}), mean dimension (D_{mean}), aggregate fractal dimension (D_f), porosity (ε), sphericity (Ψ) and density (ρ). Results show that the mean of the flocs' highest dimension (D_{max}) was 362 μm, with a maximum of 816 μm, a standard deviation of 121 μm, and a confidence interval (0.05) of 21 μm. For the flocs' lowest dimension (D_{min}), a mean of 138 μm was obtained, with a maximum of 310 μm, a standard deviation of 47 μm, and a confidence interval for the mean (0.05) of 8 μm. The average floc size obtained in the experiments was 231 μm, with a maximum of 451 μm, a standard deviation of 70 μm, and a confidence interval for the mean (0.05) of 12 μm. The three-dimensional fractal dimension (D_f) calculated per aggregate has a mean of 2.61 for the interval 2.33–2.83, indicating a variety of floc shapes, ranging from the most elongated to those close to spheres, in the limits of the interval. For the experiments, density was obtained for the flocs (ρ_{floc}) with a mean of 1,068 kg·m^{-3} within the range of 1,024–1,138 kg·m^{-3}. The mean porosity (ε) of the aggregates was 0.76 with an interval of 0.53–0.91. Sphericity (Ψ) and aspect ratio (D_{max}/D_{min}) of 0.58 and 2.62 average, respectively, showed that flocs are majority elongated structures, far from spherical.

Figure 6 shows the relationship between porosity and fractal dimension, with the more open structures ($D_f < 2.5$) having a greater porosity (>80%) than more closed

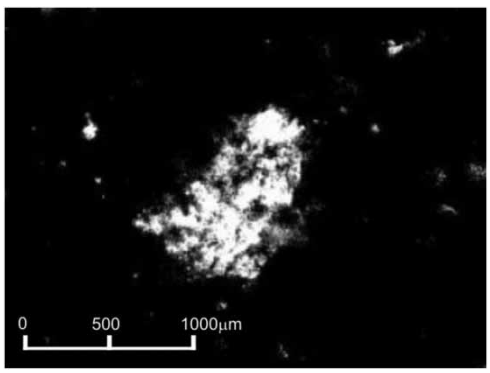

Figure 4 | Example of a porous aggregate image taken during sedimentation.

Table 1 | Descriptive statistic for aggregates' highest dimension (D_{max}), lowest dimension (D_{min}), mean dimension (D_{mean}), fractal dimension (D_f), porosity (ε), sphericity (Ψ), aspect ratio (D_{max}/D_{min}) and density (ρ)

Attribute	Average	Standard deviation	Max	Min	95%*
D_{max} (μm)	362	121	816	196	21
D_{min} (μm)	138	47	310	73	8
$D_{average}$ (μm)	231	70	451	156	12
D_f (–)	2.61	0.09	2.83	2.33	0.02
ρ_f (kg m^{-3})	1,068	22	1,138	1,024	4
ε (–)	0.76	0.07	0.91	0.53	0.01
Ψ (–)	0.58	0.14	0.97	0.14	0.02
D_{max}/D_{min}	2.62	0.67	5.14	1.53	0.12

*95% significance.

structures. To a lesser extent than shape, large size flocs have also shown greater porosity for the same fractal dimension. The average porosity found here (approximately 76%) is in agreement with Gorczyca & Ganczarczyk (1999) and Vahedi & Gorczyca (2012) for large flocs. There is no doubt that shape and porosity are dependant floc traits which may affect settling rate, however, the nonhomogeneous mass distribution and pore population within aggregate structure are also important for terminal velocity, and should be considered for further developments, as suggested by Vahedi & Gorczyca (2014).

The direct consequence of the shape and porosity relation on floc settling rates is the influences on an aggregate's density and drag. Unless water can flow through floc voids, reducing the resistance to settling, an elongated aggregate is more likely to have lower settling rates than those closer to a sphere-shape. The so-called flow-through effect is still not well understood and there is also no consensus on the contribution of permeability to the terminal velocities of porous aggregates. Whilst initially Adler (1987) showed that the effect of permeability on floc settling is minor and that it is unlikely water can flow through pores during sedimentation, nevertheless Johnson *et al.* (1996) showed the more porous the floc is, the more likely fluid can flow through it, increasing permeability and so reducing resistance to settling. In general, the literature has shown that elongated aggregates are likely to settle at lower rates than spheres and, according to Bushell *et al.* (2002), it is difficult to explain the greatly reduced resistance to settling described by Johnson *et al.* (1996).

Figure 7 shows that more spherical, less elongated aggregates (with increased D_f values) display a greater density, contributing to higher terminal velocity of aggregates. Therefore, the density of the aggregates varies inversely with porosity. If the mass was the predominant effect on floc

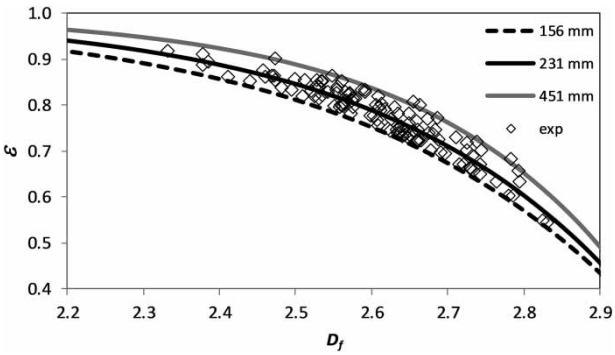

Figure 6 | Aggregate porosity ϵ (-) as a function of D_f for the minimum, average and maximum aggregate size in micrometres (μm).

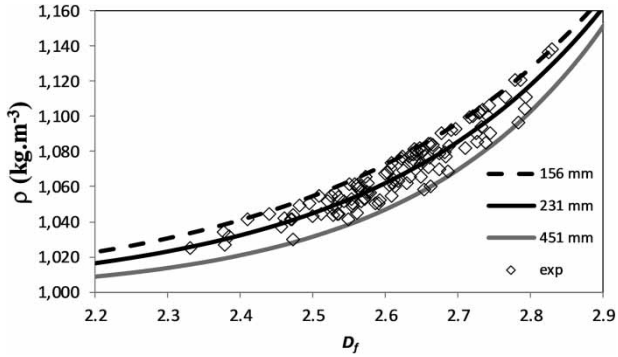

Figure 7 | Density of the aggregates ρ_f as a function of D_f for the minimum, average and maximum aggregate size in micrometres (μm).

settling velocity, compact spheres would always exhibit higher settling velocities. In fact, several researchers have shown that fractal aggregates can settle with slower velocities than those predicted by Stoke's law (Tambo & Watanabe 1979; Khelifa & Hill 2006; Jarvis *et al.* 2008; Vahedi & Gorczyca 2012).

Consequently, terminal velocities of aggregates will mostly depend upon the dual effect of porosity and density, determined to a great extent by aggregate shape, i.e fractal dimension.

Based on the experimental results, it was possible to construct a relationship between porosity (ε) and the density (ρ_f) of the aggregate (Figure S2 in the Supplementary Information and Equations (24) and (25)) such that:

$$\varepsilon = A(1 - B\rho_f) \tag{24}$$

where:

$$A = \left(1 - \frac{\rho_l}{\rho_p}\right)^{-1} \tag{25}$$

$$B = \rho_p^{-1}$$

Common practice for designers of sedimentation tanks is to adopt average floc density for perfect spheres, so that settling velocities of aggregates can be simulated using a characteristic aggregate size and Stokes' law, as Equation (21). However, results shown here suggest that flocs are elongated, porous structures, and far from spherical.

The impact of this oversimplification of floc shape is that the drag force changes as result of the cross-sectional area, thus altering the settling velocity. In general, it is supposed that deviation from sphericity will result in increasing drag, irrespective of floc orientation and permeability

(Bushell *et al.* 2002). However, Johnson *et al.* (1996) suggest that the actual drag is lower than that calculated for fractal aggregates, even when permeability is considered. Figure 8 shows calculated settling velocity for spheres and flocs (based on Equations (21) and (22) for d_p of 7.5 μm, this being median particle size by volume) against floc size for different shapes, i.e. fractal dimensions ($D_f = 3.00$ for spheres; 2.33, 2.61 and 2.83 for fractals).

Figure 8 shows that fractal aggregates of size between 100 and 300 μm settle with velocities between 0.3 and 7.9 mm/s, which is in agreement with results presented by Vahedi & Gorczyca (2012), Khelifa & Hill (2006) and Jarvis *et al.* (2008), who performed both experiments and simulations. The authors showed settling velocities varying from 0.1 to 7.1 mm/s for aggregate size between 100 and 300 μm, corroborating that the simulations presented here are within experimental measurements performed by several authors. Nevertheless, results compiled by Khelifa & Hill (2006) reveal there is considerable scatter in settling velocity of fractal aggregates, varying up to 100-fold from each other for the same floc size, possibly due to the nonhomogeneous mass distribution and pore population mentioned by Vahedi & Gorczyca (2014). Here, aggregates with a fractal dimension of 2.83 settled with higher velocities than spheres of the same size, for all ranges of floc sizes, due to the usual assumption that spherical flocs have the same density as fractal aggregates, and so less mass than aggregates of equal size.

Conversely, for aggregates with fractal dimension of 2.33 and 2.61 there is a size threshold above which fractals settle with lower velocities than those calculated using Stokes' law for compact spheres. For small floc sizes, close to the size of the primary particle ($d_f \approx d_p$), the geometric term of Equation (22) approaches the term d_f^2 from Equation

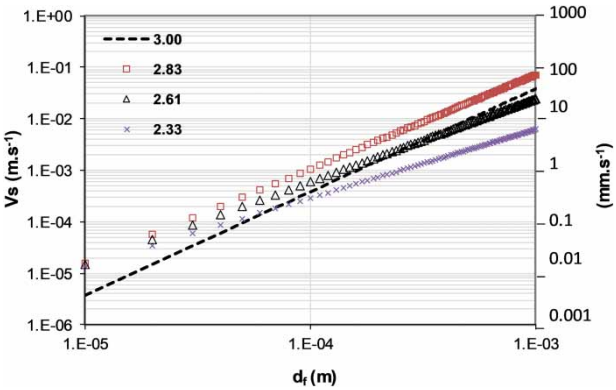

Figure 8 | Simulation of terminal velocities for Euclidean sphere (D_f of 3 and ρ_f of 1,068 kg·m^{-3}) and fractal (D_f of 2.83, 2.61 and 2.33); ρ_l of 998 kg·m^{-3}; d_p of 7.5 μm.

(21) and, therefore, the differential density between particle and liquid is the predominant driving effect over settling rate, surpassing the reduction caused by the fractal geometry. However, the differential density is not enough to surpass the reduction in the geometry term of Equation (22), caused by the low fractal dimension of elongated large aggregates. Results presented by Vahedi & Gorczyca (2012) have also shown that multi-fractal aggregates can settle with lower velocities than those predicted by the modified Stokes' law, by introducing a porous effect into the original equation. The authors simulated fractal aggregates with multi-fractal dimension varying from 2.6 to 2.7 and aggregate size less than 320 μm. In contrast, experiments carried out by Johnson *et al.* (1996) showed that settling velocities of fractal aggregates were between four and eight times greater than those predicted by Stokes' law, for aggregate size in the range of 100–1,000 μm. Here, fractal aggregates ($D_f = 2.61$, $d_f > 320$ μm) settle with lower velocities than those predicted by Stokes' law; whilst, for $D_f =$ 2.33, all aggregates of $d_f > 70$ μm and $d_p = 7.5$ μm settled below the velocity calculated by Stokes' law for spheres.

The ratio of the fractal to Euclidean velocities (Γ) is shown in Figure 9(a) for different values of the aggregates' mean equivalent diameter (d_f) in the situation ($D_f = 3.00$ for spheres; 2.33, 2.61 and 2.83 for fractals). The ratio of fractal aggregate to sphere settling velocity (the former being obtained from fractal porosity and density considerations), varied from 0.16 to 4.11 for aggregates in the range of 10 to 1,000 μm, primary particle size of 7.5 μm and three-dimensional fractal dimension between 2.33 and 2.83. This emphasizes that fractal aggregates can behave differently, settling with higher or lower velocities, compared with Stokes' law, once settling velocities of aggregates depend upon the dual effect of porosity and density, determined by the aggregate's shape. Although large elongated flocs contain higher mass, their shape results in a lower contribution of the geometric term of Equation (22) to the settling rate than small flocs. This would only be overcome if water could flow through the flocs' pores whilst settling, as a result of macro-pore distribution within the aggregates, as mentioned by Vahedi & Gorczyca (2012). Again, there is no consensus about the permeability effect on settling rate of fractal aggregates, and despite the fact that permeability was not considered here for modelling, the findings are in agreement with a wide range of experiments, like those performed by Vahedi & Gorczyca (2012) and Johnson *et al.* (1996), for instance.

On the other hand, if primary particle size is changed, results vary for the same fractal geometry. Figure 9(b)

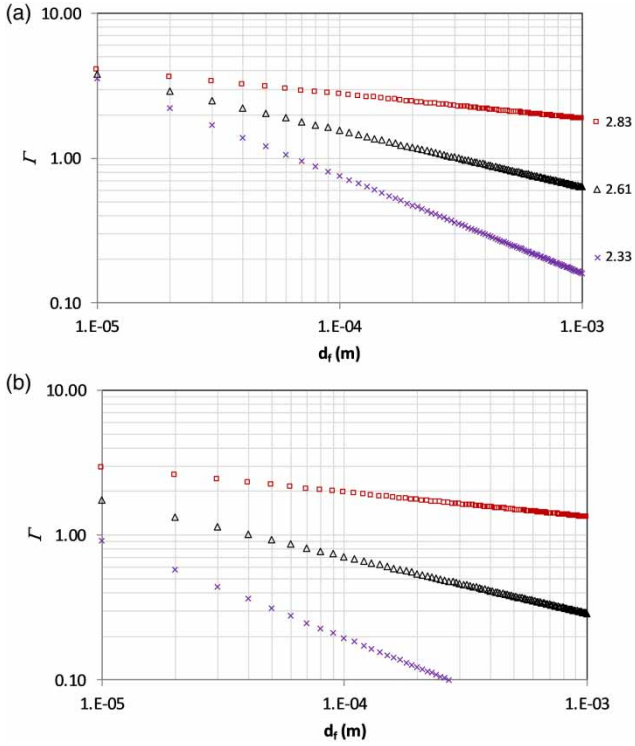

Figure 9 | Fractal to Euclidean velocities ratio (Γ) for D_f of 2.83, 2.61 and 2.33: (a) d_p of 7.5 μm; (b) d_p of 1.0 μm.

shows the effect of primary particle size (d_p) on Γ. Results were taken following the same procedures used for Figure 9(a), and it is clear that the d_p of 1.0 μm can change the ratio of fractal aggregate to sphere settling velocity markedly to values between 0.04 and 2.92, i.e. in a lower range when compared with the d_p of 7.5 μm. For the same fractal dimension, the lower the d_p, the higher the porosity and, therefore, the lower the density, thus affecting the mass contribution over the terminal velocities of the aggregates. Further, the results showed all velocities simulated for fractal dimension of 2.33 were far lower than those predicted by Stokes' law for spheres ($\Gamma < 1$), and only aggregates with size lower than 40 μm settled with higher velocities than Stokes' law for spheres when a fractal dimension of 2.61 was simulated, although, Γ was always higher than 1 for a fractal dimension of 2.83.

Whether lower or higher, simulations have shown that settling velocities of fractal aggregates can be very different from those predicted by spheres using Stokes' law. The factors affecting settling velocities of fractal aggregates depend upon size, shape, porosity, permeability, and primary particle size, and are far more complex than assumed by Stokes' law for spheres. Results presented in this paper have shown that settling velocities may vary strongly when floc shape changes from spherical to fractal aggregates, and the accuracy of predictions varies with floc size, fractal dimension and primary particle size. In practice, settling velocities of flocs are a function of floc size and fractal dimension, which are controlled by coagulation flocculation units.

CONCLUSIONS

In this study, the porosity and density of aggregates formed after the flocculation of water containing kaolin were calculated using fractal dimension, and the terminal velocities of the Euclidean sphere and of the fractal aggregates were determined using images of a series of 118 flocs measured individually.

Settling was not used as a means to characterize aggregates' behaviour, but image analysis was used instead. Therefore, the simulations here performed were derived from aggregates' characteristics taken by image analysis, to input data into both Stokes' equation and the modified equation, based on fractal geometry. Findings are in agreement with a wide range of aggregates' traits and settling rates reported in the literature, confirming that the results are reliable.

A consistent increase of aggregate porosity with decrease of fractal dimension was observed, and the opposite was observed for the density of aggregates. Therefore, more spherical aggregates display a greater density, contributing to a higher terminal velocity of aggregates.

It was found that fractal aggregates can behave differently, settling with higher or lower velocities, compared with Stokes' law, once settling rates of aggregates depend upon the dual effect of porosity and density, determined by the aggregate's size and shape. For small floc sizes, close to the size of the primary particle ($d_f \approx d_p$), the differential density between particle and liquid is the dominant effect on settling rate, surpassing the geometry reduction yielded by fractal aggregates. The opposite was observed for large fractal aggregates, where the differential density was not big enough to surpass the reduction caused by the low fractal dimension of elongated aggregates.

The results obtained differ from other work in the field by calculating settling velocities from fractal dimension and demonstrated the importance of advancing the analysis of particles considering their sizes and shapes beyond those described by Euclidean geometry. Specifically, applying fractal geometry to determine the porosity and density of the flocs is an important evaluation tool, with far-reaching implications for sedimentation tank design and operation.

ACKNOWLEDGEMENTS

Rodrigo B. Moruzzi is grateful to São Paulo Research Foundation (Fundação de Amparo à Pesquisa do Estado de São Paulo – FAPESP) Grant 2017/19195-7 for financial support and to CNPq for the fellowship Grant 301210/2018-7.

SUPPLEMENTARY MATERIAL

The Supplementary Material for this paper is available online at https://dx.doi.org/10.2166/wst.2020.171.

REFERENCES

Adler, P. M. 1987 Hydrodynamic properties of fractal flocs. *Faraday Discussions of the Chemical Society* **83**, 145–152.

Aparicio, P., Pérez-Bernal, J. L., Galán, E. & Bello, A. 2004 Kaolin fractal dimension. Comparison with other properties. *Clay Minerals* **39** (1), 75–84.

Bache, D. H., Rasool, E., Moffatt, D. & McGilligan, F. J. 1999 On the strength and character of alumino-humic flocs. *Water Science and Technology* **40** (9), 81–88.

Bushell, G. C., Yan, Y. D., Woodfield, D., Raper, J. & Amal, R. 2002 On techniques for the measurement of the mass fractal dimension of aggregates. *Advances in Colloid and Interface Science* **95** (1), 1–50.

Chakraborti, R. K. & Kaur, J. 2014 Noninvasive measurement of particle-settling velocity and comparison with Stokes' law. *Journal of Environmental Engineering* **140** (2), 04013008.

Chakraborti, R. K., Atkinson, J. F. & Van Benschoten, J. E. 2000 Characterization of alum floc by image analysis. *Environmental Science and Technology* **34** (18), 3969–3976.

Chakraborti, R. K., Gardner, K. H., Atkinson, J. F. & Van Benschoten, J. E. 2003 Changes in fractal dimension during aggregation. *Water Research* **37** (4), 873–883.

de Oliveira, A. L., Moreno, P., da Silva, P. A. G., De Julio, M. & Moruzzi, R. B. 2015 Effects of the fractal structure and size distribution of flocs on the removal of particulate matter. *Desalination and Water Treatment* **57** (36), 16721–16732.

Gorczyca, B. & Ganczarczyk, J. 1999 Structure and porosity of alum coagulation flocs. *Water Quality Research Journal* **34** (4), 653–666.

Gregory, J. 1997 The density of particle aggregates. *Water Science and Technology* **36** (4), 1–13.

Gregory, J. 2009 Monitoring particle aggregation processes. *Advances in Colloid and Interface Science* **147–148**, 109–123.

He, W., Nan, J., Li, H. & Li, S. 2012 Characteristic analysis on temporal evolution of floc size and structure in low-shear flow. *Water Research* **46** (2), 509–520.

Jarvis, P., Parsons, S. A., Henderson, R., Nixson, N. & Jefferson, B. 2008 The practical application of fractal dimension in water treatment practice – the impact of polymer dosing. *Separation Science and Technology* **43** (7), 1785–1797.

Johnson, C. P., Li, X. & Logan, B. E. 1996 Settling velocities of fractal aggregates. *Environmental Science & Technology* **30** (6), 1911–1918.

Khelifa, A. & Hill, P. S. 2006 Models for effective density and settling velocity of flocs. *Journal of Hydraulic Research* **44** (3), 390–401.

Kim, S. H., Moon, B. H. & Lee, H. I. 2001 Effects of pH and dosage on pollutant removal and floc structure during coagulation. *Microchemical Journal* **68** (2–3), 197–203.

Li, T., Zhu, Z., Wang, D., Yao, C. & Tang, H. 2006 Characterization of floc size, strength and structure under various coagulation mechanisms. *Powder Technology* **168** (2), 104–110.

Logan, B. E. & Kilps, J. R. 1995 Fractal dimensions of aggregates formed in different fluid mechanical environments. *Water Research* **29** (2), 443–453.

Moruzzi, R. B., de Oliveira, A. L., da Conceição, F. T., Gregory, J. & Campos, L. C. 2017 Fractal dimension of large aggregates under different flocculation conditions. *Science of the Total Environment* **609**, 807–814.

Moruzzi, R. B., da Silva, P. G., Sharifi, S., Campos, L. C. & Gregory, J. 2019 Strength assessment of Al-humic and Al-kaolin aggregates by intrusive and non-intrusive methods. *Separation and Purification Technology* **217**, 265–273.

Tambo, N. & Watanabe, Y. 1979 Physical characteristics of flocs – I. The floc density function and aluminium floc. *Water Research* **13** (5), 409–419.

Vahedi, A. & Gorczyca, B. 2012 Predicting the settling velocity of flocs formed in water treatment using multiple fractal dimensions. *Water Research* **46** (13), 4188–4194.

Vahedi, A. & Gorczyca, B. 2014 Settling velocities of multifractal flocs formed in chemical coagulation process. *Water Research* **53**, 322–328.

Xu, W., Gao, B., Yue, Q. & Wang, Y. 2010 Effect of shear force and solution pH on flocs breakage and re-growth formed by nano-Al_{13} polymer. *Water Research* **44** (6), 1893–1899.

Xu, W., Gao, B., Yue, Q. & Bo, X. 2011 Influence of pH on flocs formation, breakage and fractal properties – the role of Al_{13} polymer. *Journal of Water Sustainability* **1** (1), 45–57.

Yukselen, M. A. & Gregory, J. 2004 The reversibility of floc breakage. *International Journal of Mineral Processing* **73** (2–4), 251–259.

Zbik, M. & Smart, R. S. C. 1998 Nanomorphology of kaolinites: comparative SEM and AFM studies. *Clays and Clay Minerals* **46** (2), 153–160.

First received 17 February 2020; accepted in revised form 31 March 2020. Available online 10 April 2020